# Adaptive Wave Reconstruction Through Regulated-BMFLC for Transparency-Enhanced Telerobotics Over Delayed Networks

Navid Feizi, *Graduate Student Member, IEEE*, Rajni V. Patel, *Life Fellow, IEEE*, Mehrdad R. Kermani, *Member, IEEE*, and S. Farokh Atashzar, *Senior Member, IEEE* 

Abstract—Bilateral telerobotic systems have attracted a great deal of interest during the last two decades. The major challenges in this field are the transparency and stability of remote force rendering, which are affected by network delays causing asynchrony between the actions and the corresponding reactions. In addition, the overactivation of stabilizers further degrades the fidelity of the rendered force field. In this article, a real-time frequency-based delay compensation approach is proposed to maximize transparency while reducing the activation of the stabilization layer. The algorithm uses a regulated bound-limited multiple Fourier linear combiner to extract the dominant frequency of force waves. The estimated weights are used in conjunction with the relatively phaselead harmonic kernels to reconstruct the signal and generate a compensated wave to reduce the effect of the delay. The reconstructed force will then pass through a modulated time-domain passivity controller to guarantee the stability of the system. We will show that the proposed technique will reduce the force-tracking error by 40% and the activation of the stabilizer by 79%. It is shown, for the first time, that through the utilization of online adaptive frequency-based prediction, the asynchrony between transmitted waves through delayed networks can be significantly mitigated

Manuscript received 31 October 2021; accepted 11 February 2022. Date of publication 19 April 2022; date of current version 4 October 2022. This paper was recommended for publication by Associate Editor Chenguang Yang and Editor Eiichi Yoshida upon evaluation of the reviewers' comments. The work of Navid Feizi and Rajni V. Patel was funded by the Natural Sciences and Engineering Research Council of Canada under Grant #RGPIN-1345 (awarded to RVP) and the Tier-1 Canada Research Chairs Program (RVP). The work of Mehrdad R. Kermani was supported by the Natural Sciences and Engineering Research Council of Canada under Grant #RGPIN-06253. The work of S. Farokh Atashzar was supported by the U.S. National Science Foundation under Grant #2037878 and Grant #2121391. (Corresponding author: S. Farokh Atashzar.)

Navid Feizi is with the Canadian Surgical Technologies and Advanced Robotics (CSTAR), Lawson Health Research Institute, London, ON N6A 5A5, Canada, and also with the School of Biomedical Engineering, Western University, London, ON N6A 3K7, Canada (e-mail: nfeizi@uwo.ca).

Rajni V. Patel is with the Canadian Surgical Technologies and Advanced Robotics (CSTAR), Lawson Health Research Institute, London, ON N6A 5A5, Canada, and also with the Department of Electrical and Computer Engineering, School of Biomedical Engineering, Department of Surgery, and Department of Clinical Neurological Sciences, Western University, London, ON N6A 5B9, Canada (e-mail: rvpatel@uwo.ca).

Mehrdad R. Kermani is with the Department of Electrical and Computer Engineering, Western University, London, ON N6A 5B9, Canada (e-mail: mkermani@eng.uwo.ca).

S. Farokh Atashzar is with the Department of Mechanical, Aerospace Engineering, Department of Electrical, Computer Engineering, and Department of Biomedical Engineering, New York University (NYU), New York, NY 10003 USA, and also with the NYU WIRELESS and NYU CUSP, New York, NY 11201 USA (e-mail: f.atashzar@nyu.edu).

Color versions of one or more figures in this article are available at https://doi.org/10.1109/TRO.2022.3158195.

Digital Object Identifier 10.1109/TRO.2022.3158195

while stability can be guaranteed with less activation of the stabilization layer.

Index Terms—Adaptive filters, stability, telerobotics, transparency.

#### I. INTRODUCTION

ELEROBOTIC systems have extended the sensorimotor competence of human beyond physiological and physical barriers, such as access, scale, and safety concerns in hazardous environments. The technology has allowed human operators to function remotely, also where the performance more than natural ranges is needed while allowing for amplification of power and precision. The versatility of telerobotic systems has attracted a great deal of interest in the industrial sector and in space and marine applications [1]. Later, the technology was adopted in medical domain, such as surgery and rehabilitation [2]. In addition, it is worth mentioning that the COVID-19 pandemic has shown a greater need for telerobotics, especially in clinical domain, to minimize the risk of infection transfer (please see [3], [4], and references therein).

A successful example of leader–follower robotic teleoperation is the da Vinci surgical system. However, haptic feedback is not enabled yet in practical applications of telerobotics, while the use of it is known to be an imperative need for telephysical medicine, including telerehabilitation and telesurgery [5], [6].

One of the major challenges with force reflection in hapticsenabled bilateral teleoperated systems is to provide transparent force feedback while guaranteeing stability. In this regard, new mechanical designs of actuators for haptic devices have been investigated in [7] and [8]. In addition, several control architectures have been proposed to enhance the transparency for a given haptic system. In this regard, an ideal teleoperation system should reflect environmental forces to the operator in order to accurately enable the remote perception of the environmental dynamics in a stable manner [9].

In order to close the loop of teleoperation, several telerobotic architectures have been proposed in the past two decades. A two-channel architecture was proposed, as the very first bilateral solution without providing pure transparency. Canceling the interactional dynamics of the robots in the teleoperated system, the Lawrence's four-channel (LFC) design was proposed as the first transparent teleoperation system [9]. LFC was modified to

1552-3098 © 2022 IEEE. Personal use is permitted, but republication/redistribution requires IEEE permission. See https://www.ieee.org/publications/rights/index.html for more information.

improve robustness against model uncertainties by introducing local force controllers in the design of the teleoperation [10]. In the extended LFC (ELFC) architecture, one of the feedforward force channels is eliminated without affecting transparency. This simplification addressed the complexity of the system by reducing the number of channels to three [11]. In [12], a modified ELFC (MELFC) was proposed in which the follower coordinating feedforward module was also eliminated, leading to a more simplified control architecture by reducing the number of channels to two (the minimum possible), while enhancing the transparency.

Although the abovementioned control architectures are stable under ideal (delay-free) communication, they compromise the stability in a delayed network [12]. The reason is that according to the absolute stability theory, an ideally-transparent bilateral teleoperation system is marginally stable [13]. Thus, even a small delay, unmodeled dynamics, or sampling discretization may affect system stability [14].

The stability of the bilateral teleoperated systems has been investigated extensively in the literature, mostly using the passivity control theory and the small gain theory. This includes our recent efforts published in [15]–[18]. Wave variable control (WVC) is one of the very first proposed methods in the literature designed based on the passivity theory to compensate for the nonpassive behavior of the communication delay. Implementation of the WVC for two-channel and four-channel teleoperation architectures can be found in [20]–[22]. However, WVC imposes a considerable cost regarding degraded transparency due to the conservative design. A different reputable stabilizer is the time-domain passivity approach (TDPA), which utilizes a virtual variable-damping factor based on the observation of energy flow of the system, while taking into account the stability condition based on the passivity control theory [23], [24]. Similar to WVC and almost all stabilization schemes, TDPA also has detrimental effect on the transparency of the rendered force field.

A large body of research has been conducted around improving the performance of TDPA stabilizers. Two-port TDPA was introduced in [25] to reduce the conservatism by considering bidirectional energy flow through communication channels. The conservatism is further reduced in a two-port TDPA by considering the reflected energy of the follower robot controller in the passivity observer formulation [26]. However, position drift issue rises in two-port stabilizers due to the velocity modification [18]. Position drift compensator was proposed in [27] and [28] to address the mentioned issues with a two-port TDPA. In another attempt, a transparency-oriented approach has been implemented for the passivity control layer in teleoperation systems to improve transparency [29]–[31].

Regarding performance improvement in a one-port TDPA, power-based TDPA is proposed in the literature to provide smoother force and velocity profiles, but it may result in a more conservative formulation by overcompensating the negative power packets [32]. In addition to the above, a modulated time-domain passivity controller (M-TDPC) is proposed recently by the authors to also address the problem of nonpassive environments, which is the second source of nonpassivity (besides communication delay) and can challenge the performance of several conventional passivity-based stabilizers. M-TDPC

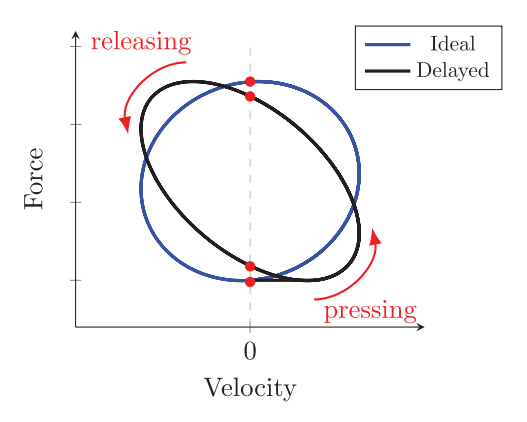


Fig. 1. Force versus velocity diagram for delay-free (blue) and delayed (black) teleoperation. Positive velocity shows the pressing phase and negative velocity shows the releasing phase. Red dots show the instances of phase change.

significantly reduces the conservatism of bilateral teleoperation by embedding the estimation of the lower bound of the excess of passivity (EoP) of the human biomechanics into the control formulations [15]. EoP in this context quantifies the ability of human biomechanics to absorb the mechanical energy during human-robot interaction. Variable structure passivity signature control (VSPSC) is proposed recently to further reduce the complexity of nonlinear formulation, and result in smoother outcomes in the power domain considering not only the lower bound, but also the variability of the EoP of the user's biomechanics [16]. The VSPSC design was extended by introducing the concept of windowed energy, which provides the designer with flexibility to switch smoothly between power and energy domains. It benefits from the features of both domains and reduces the drawbacks of pure energy-domain and pure-powerdomain designs [17].

Despite the extensive literature on guaranteeing the stability and transparency of teleoperated systems (summarized above), relatively low attention has been devoted to counteracting the reduced transparency caused by the network delay and the corresponding asynchrony between action-reaction couples of information. It should be noted that even, in the best-case scenario, when a delayed teleoperation system remains stable without the intervention of the stabilizer, there is still a misperception of the environmental dynamics because of the lagged-rendered reaction forces, which affect the feel of causality of the user. Fig. 1 shows the visualization of the effect of delay between motion and force in a pressing-releasing task in contact with a viscoelastic wall. Positive velocity is associated with the pressing phase, negative velocity is associated with the releasing phase, and red dots show the onset of phase change. The figure graphically demonstrates that in the delay-free scenario (shown in blue), the reflected force increases with the start of the pressing phase and decreases right after the start of the releasing phase. This leads to the formation of a circular graph. However, by introducing delay into the system (shown in black), it can be seen that the reflected force continues to increase even after the start of the releasing phase, and in the next cycle, the force continues to decrease after the onset of the pressing phase. The introduced phase lag in the force signal results in the skewness of the relationship between force and velocity, affecting causality. This phenomenon, which only happens because of the communication delay, causes serious misperception of the environmental impedance. Detailed relevant discussion can be found in [33].

In this article, we propose a novel real-time frequency-based model-free (i.e., not based on a model of the environment or the operator) delay compensation to address the transparency degradation issue due to asynchrony between action—reaction couples in a haptics-enabled telerobotic over delayed networks. The difference between this method and other transparency improvement methods is that it reduces the existing delay by predicting actions in the signal, which improves transparency along with causality. The proposed algorithm can be added as a modular component to any state-of-the-art stabilization algorithm, including energy tank-based, as it will directly optimize the flow of the wave information by compensating for the effect of the delay. So, it can be expected that the activation of the stabilizer will be lower; thus, less deterioration of the transparency can be expected.

The contributions of this article are as follows.

- A novel signal predictor based on the signal modeling with a regulated bound-limited multiple Fourier linear combiner (R-BMFLC) is proposed. In the predictor, the frequency decomposed signal model is used in conjunction with phase-lead harmonic kernels to predict nondelayed signals and compensate for communication delay.
- 2) The force transparency degradation problem due to asynchrony between action–reaction couples and stabilizer's activation in delayed haptics-enabled telerobotic is addressed. This has been done by mitigating the effect of the introduced phase lag by the network delay, which also leads to minimizing the signal modifications by the stabilizer in the system. This provides the operator as close a feel as possible of the environmental impedance.
- 3) The performance of the system is evaluated through experimental validation and a systematic grid simulation showing that the proposed approach results in 40% reduction of force modification and 79% reduction of activation of the stabilizer.

The rest of this article is organized as follows. In Section II, the preliminaries regarding the bound-limited multiple Fourier linear combiner (BMFLC) are explained. In Section III, the structure of the delay compensator model, implementation in unilateral teleoperation, and required modifications for performance improvement are explained. In Section IV, optimal design parameters and a method for optimizing them are presented. Section V represents the delay compensator along with a stabilizer to guarantee stability in bilateral teleoperation. In Section VI, experimental results and discussion for unilateral and bilateral teleoperation with delay compensator are presented. Finally, Section VII concludes this article.

# II. PRELIMINARIES: SIGNAL MODELING WITH BMFLC

In this article, BMFLC is generalized for frequency modeling of human hand motion signals used to compensate for the delay. Conventional BMFLC has been used in [34]–[37] for real-time signal filtering due to the corresponding low-latency in several applications, such as modeling of physiological hand tremor of

surgeons. In addition, recently, we have enhanced the design of BMFLC to extract the dominant frequency of human hand motion, relaxing the assumption of periodic behavior of the signal and enriching the memory of the algorithm to separate the low-frequency voluntary from the high-frequency pathological motions [38]. The preliminaries regarding BMFLC are given as follows.

#### A. BMFLC Concepts

In the BMFLC formulation, the harmonic model of the signal is tracked based on the truncated Fourier series as follows:

$$y(t) = \sum_{i=0}^{\beta(\omega_b - \omega_a)} a_i \sin\left(\left(\omega_a + \frac{i}{\beta}\right)t\right) + b_i \cos\left(\left(\omega_a + \frac{i}{\beta}\right)t\right)$$
(1)

where  $[\omega_a, \ \omega_b]$  is the frequency window of estimation,  $\beta$  is the number of harmonics considered for unit of frequency (representing the frequency resolution of the model), and  $a_i$  and  $b_i$  are the coefficients of the Fourier model to be estimated adaptively. The model shown in (1) can be rewritten as

$$y(t) = W(t)^T X(t) \tag{2}$$

where W(t) is the vector of Fourier model coefficients (weights) at time t, and X(t) is the vector of harmonic kernels as follows:

$$X(t) = \begin{cases} 1 & k = 0\\ \sin(\omega_k t) & k = 1, 2, \dots, L+1\\ \cos(\omega_k t) & k = L+2, L+3, \dots, 2L+1 \end{cases}$$
(3)

where L is the total number of harmonics, which is  $\beta \times (\omega_b - \omega_a)$ . A constant is included in the harmonic kernels to take into account the zero frequency components. Having the input signal d(t) and estimated signal y(t), the BMFLC estimation error is defined as

$$e(t) = d(t) - y(t). (4)$$

The generation of the harmonic model of the signal will be achieved through minimizing the estimation error e(t) in real-time. In [37], the least mean squares (LMSs) were commonly used for BMFLC to optimize the linear regression model shown in (4) and to estimate the coefficients. However, the slow convergence of the LMS can result in significant estimation errors in the implementation of the proposed delay compensator. Therefore, other methods, such as recursive least square (RLS) [39] and Kalman filter (KF) [40], have also been used in the literature and by our team. In this article, we use an enhanced formulation of RLS (explained later) for optimization of the regression (see Fig. 2) to achieve faster and more reliable convergence and to enhance estimation accuracy while securing a relatively low computational cost [39].

Visualization of the formulation of the BMFLC-RLS signal decomposer is shown in Fig. 2. The signal decomposer block takes the desired signal as the input and returns Fourier coefficients in real-time. An initial estimation of the desired signal is generated using the harmonic kernels and the initial values of the Fourier model coefficients. The estimation error signal goes to the RLS optimizer for online optimization of the Fourier model coefficients for the next sample.

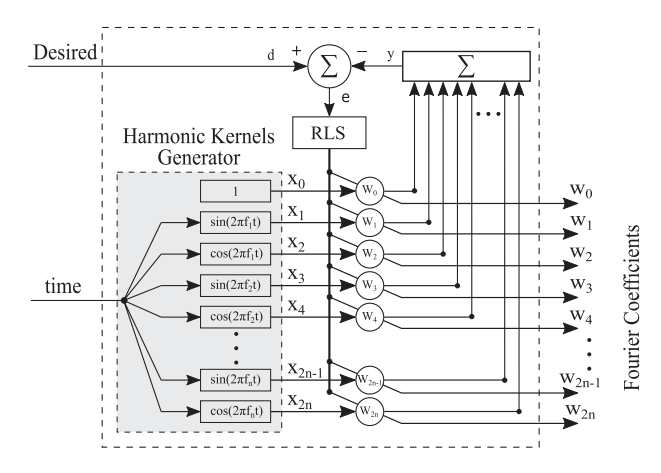


Fig. 2. BMFLC-RLS signal decomposer.

It should be noted that the model used in BMFLC can significantly grow depending on the chosen frequency resolution. In the context of haptics rendering, lower computational cost is of prominent importance because calculations need to be done in real-time with a relatively high sampling rate. We have previously discussed that the high computation cost of the KF for BMFLC may challenge real-time calculations for high-frequency resolution in haptics-rendering applications (depending on the speed of the processor used) [38]. The LMS and RLS methods take  $\mathcal{O}(N)$  operations; however, KF takes  $\mathcal{O}(3\ N^2)$  operations per estimation [41].

It should also be noted that the cost function of RLS is defined based on the least-square criterion as

$$J(t) = \sum_{i=0}^{t} \lambda^{t-i} [e(i)]^2$$
 (5)

where J(t) is the cost function at time t,  $\lambda$  is the exponential forgetting factor integrated into the RLS algorithm, and e is the BMFLC estimation error.

The RLS algorithm derives as

$$W(t + \Delta t) = W(t) + [R(t)]^{-1}X(t)e(t)$$
(6)

where

$$R(t) = \lambda R(t - \Delta t) + X(t)X^{T}(t) \tag{7}$$

where R(t) is an estimation of the correlation matrix at time t,  $\lambda$  is the exponential forgetting factor, e is the BMFLC estimation error, and  $\Delta t$  is the sample time [42].

The exponential forgetting factor  $\lambda$  plays an important role in RLS implementation for system identification. A  $\lambda$  close to one increases the stability of the algorithm; however, it makes the algorithm slow, leading to reduced tracking accuracy. On the other hand, a  $\lambda$  close to zero increases the sensitivity of the algorithm to the recent values thereby increasing the tracking accuracy, but with higher misadjustment that may affect stability. Thus, the exponential forgetting factor has to be tuned precisely for high accuracy estimation. More details can be found in [43].

Remark 1: In signal modeling with BMFLC, the signal is decomposed into Fourier coefficients (i.e., the weights vector) and harmonic kernels (i.e., the reference vector). The Fourier

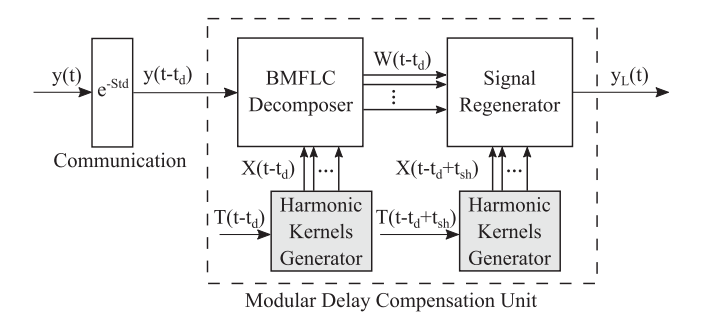


Fig. 3. One-port BMFLC lead unit. y(t) is the desired signal,  $y(t-t_d)$  is the delayed signal after communication, and  $y_L(t)$  is the compensated signal.

coefficients are time-varying weights, which are estimated by the RLS algorithm in real-time. This is further discussed later in this article since conventional RLS assumes a constant model (though there are some variations, which provide flexibility). The harmonic kernels are comprised of orthogonal sinusoidal signals with fixed amplitude and frequencies. Knowing the frequency window  $[\omega_a,\ \omega_b]$  and the number of harmonics  $\beta$ , which are constant parameters, the harmonic kernels can be regenerated in the signal reconstructor without having access to the actual harmonic kernels that have been used in the signal decomposer. This is used in conjunction with the Fourier coefficients W to reconstruct the input signal in the regenerator.

#### III. DELAY COMPENSATION BASED ON R-BMFLC-RLS

In this section, a model-free delay compensation method is proposed to counteract the communication delay. The proposed BMFLC delay compensator works based on the idea of the reconstruction of the signal using the estimated Fourier coefficients in conjunction with a *lead phase-based* harmonic kernels (harmonic kernels with phase lead with respect to the corresponding phase of the Fourier coefficients). The manipulation of the relative phase of the harmonics affects the phase of the reconstructed signal and reduces the lag caused by the delay. In other words, shifting the harmonics forward in time, with respect to the corresponding Fourier coefficients, results in an estimation of time-shifted reconstructed signal. This idea can be implemented in two different configurations, each has specific advantages.

#### A. One-Port Delay Compensation Unit

In this configuration, all the components of the delay compensator, including signal decomposer and signal regenerator, are encompassed in a single unit on the follower side (see Fig. 3); therefore, the BMFLC decomposes the delayed signal. As described in Section II, the regeneration of the harmonics in the signal regenerator allows manipulation of the phase of the harmonic kernels to compensate for the delay. Therefore, the required relative phase lead of the harmonic kernels provides by the time feed of the second harmonic kernels generator. Thus, multiplication of the estimated Fourier coefficients with phase-based lead harmonic kernels (not the original harmonic kernels) results in the reconstruction of a phase-based lead estimation of the input signal. The math is explained as follows

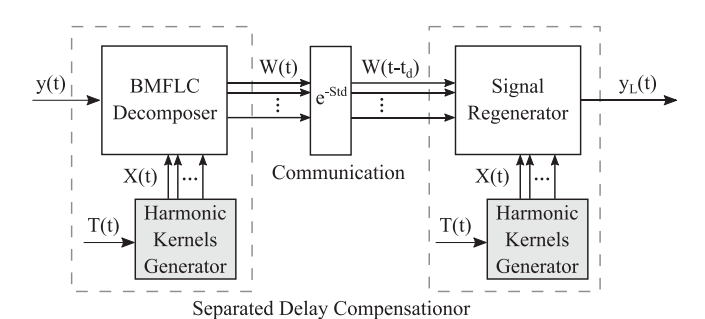


Fig. 4. Two-port BMFLC delay compensator. y(t) is the desired signal and  $y_L(t)$  is the compensated signal.

and conceptualized in Fig. 3:

$$y_L(t) = W(t - t_d)^T X(t - t_d + t_{sh})$$
 (8)

where  $t_{\rm sh}$  is an estimated lower bound of the delay, which is used as the time shift that has been added to the harmonic kernels in the harmonics regenerator, and  $t_d$  is the actual network delay.

Remark 2: If  $t_{\rm sh}$  is equal to  $t_d$ , the model compensates for the phase lag introduced to the harmonic kernels due to network delay. Various network delay measurement methods, such as the global-positioning system and IEEE 1588 standard synchronization, autoregressive, and neural network-based model, have been proposed in [44]–[47]. However, it is often not trivial to have the exact value. In this article, we assume an estimated lower bound, which can be achieved in practical applications. The more accurate the estimate is, the higher the transparency. It should be noted that due to the modular design of this article, the force feedback is passed through a stabilizer, which guarantees the stability of the system regardless of the changes of transparency. Using the approach proposed here, the effect of the time delay for each kernel can be directly calculated, and therefore, the effect of delay-induced phase lags on the regenerated harmonic kernels is significantly reduced, and thus, the effect of the delay is also reduced significantly for the reconstructed signal  $(y_L(t))$ when compared with the original delayed signal  $(y(t-t_d))$ .

# B. Two-Port Delay Compensator

In this configuration, the signal decomposer unit is placed on the leader side and the signal regenerator is on the follower side, separated by the communication channel. Thus, the BMFLC decomposes the nondelayed signal, and the estimated Fourier coefficients (not the actual signal) are sent to the follower through the communication channel. The signal regenerator estimates the signal using the delayed Fourier coefficients in conjunction with the same harmonic kernels, which were utilized in signal decomposition (see Fig. 4). The equation for this system is

$$y_L(t) = W(t - t_d)^T X(t)$$
(9)

which is a special case of (8) when  $t_{sh}$  is equal to  $t_d$ .

A significant benefit of the two-port configuration is that the phase lead of the harmonic kernels with respect to the Fourier coefficients automatically applies equal to the phase lag due to delay. Therefore, estimation of the network delay is not required. In this configuration, the signal decomposer unit and

the signal regenerator unit have to be synchronized. This can be easily done by initializing both units at the same time. The limitation of this implementation in comparison to the one-port delay compensation is that the  $t_{\rm sh}$  is intrinsically equal to  $t_d$ , disabling manipulation of the relative phase of the harmonic kernels with respect to the Fourier coefficients (the benefits of this are explained in Section IV).

Remark 3: It should be noted that under a hypothetical ideal condition when the Fourier coefficients of the input signal are constant, both approaches proposed above can completely compensate for the delay since it decomposes the signal into harmonics and applies the corresponding phase shift compensation (which is different for different kernels under the same time delay) to each kernel. However, in practice, even though the natural frequency of human hand motion is typically below 3 Hz [48], the Fourier coefficient may still slowly change. As a result, due to the nonperiodic behavior of the motion, even though we can track the Fourier coefficient using the technique proposed here, it is not possible to perfectly compensate for the effect of delay. However, the corresponding effect can be significantly minimized depending on the accuracy of the estimate of the time delay and adjustment of the compensation factor (as shown in the results) in one-port implementation.

In this article, we have revisited the conventional formulation of BMFLC by changing the LMS core for estimation and conduction an optimization step to find the most optimal settings of the hyperparameters. The optimization is conducted since for any adaptive filtering (such as the one utilized here), the choice of hyperparameters can be very critical in the resulting performance. In the literature, this is often left for the designer to choose.

Regarding the adaptive core utilized in this article, we applied following two major changes to the conventional choice utilized in the literature for BMFLC.

- 1) Utilization of the RLS formulation with an embedded vector of forgetting factors to follow the nonperiodic changes of the Fourier coefficients.
- 2) Applying a regularization factor to the cost function of RLS, which enhances the convergence of the estimated coefficients as explained further.

# C. Forgetting Factors

The conventional truncated Fourier series formulation of the BMFLC utilizes an infinite memory of the input signal, which is suitable only for periodic signals. However, if the frequency of the signal changes over time, more weights should be considered for recent information. Therefore, to perform real-time estimations of the signal relaxing the assumption of periodic behavior, a forgetting factor of  $\alpha$ , which continuously adjusts Fourier coefficient update dynamics, is considered to improve (6). Thus, (6) is modified as follows:

$$W(t + \Delta t) = \alpha W(t) + [R(t)]^{-1} X(t) e(t).$$
 (10)

The sliding memory window, defined by  $\alpha$  in (10), mitigates the effect of old history of the signal and allows the model to focus on recent behaviors. Lower values of  $\alpha$  resemble faster

forgetting dynamics of the memory. In other words,  $\alpha$  defines the pole of the dynamics of the forgetting memory, and it can be chosen based on the duration of the needed memory as

$$\alpha = \sqrt[q]{\rho}, \text{ and } \gamma = \frac{1}{\Delta t} T_p$$
 (11)

where  $T_p$  is the width of the memory window,  $\rho$  is the minimum gain within the time window, and  $\Delta t$  is the sample time.

Remark 4: Although a forgetting factor  $\lambda$  is classically integrated into the original RLS algorithm as shown in (7),  $\lambda$  only mitigates the effect of the history on the correlation matrix R. It, therefore, does not address the abovementioned issue. Thus, introducing the model forgetting factor  $\alpha$  is necessary, despite using  $\lambda$ .

#### D. Regularization

Adding forgetting factors  $\alpha$  and  $\lambda$  provides flexibility to the changes in the model. However, since they allow the model to have variable Fourier coefficients, the size of the solution space is infinity. In order to force the model to reduce the size of the solution space and minimize the variation of the estimated coefficient, a regularization term is added to the cost function of the RLS algorithm, reducing the sensitivity in the system to the changes of the frequency of the reference signals by pushing the weights to remain small in the multiobjective cost function [49]. The formulation of the R-BMFLC decomposer is

$$J(t) = \sum_{i=0}^{t} \lambda^{t-i} [e(i)]^2 + \delta ||W(t)||_2$$
 (12)

where  $\delta$  is the regularization parameter and other parameters are as defined previously.

Based on the regulated cost function given in (12), the RLS algorithm can be calculated as

$$W(t + \Delta t) = \alpha W(t) + [R(t) + \delta I]^{-1} X(t) e(t)$$
 (13)

where R(t) is the correlation matrix, as mentioned in (7).

# IV. OPTIMIZING THE DELAY COMPENSATOR PARAMETERS

As explained in Section III, the proposed R-BMFLC model has several hyperparameters that need to be designed for high accuracy. The choice of  $\beta$  and  $\delta$  have been discussed in the literature to accurately model human hand motions [38]. However, the following hyperparameters, which are specifically proposed in this article, should be automatically designed to secure a high performance for the motion analyzer. The aforementioned parameters (to be designed) are as follows.

- 1) The maximum bound of harmonic kernels frequency window  $\omega_b$ .
- 2) The forgetting factor of correlation matrix  $\lambda$ .
- 3) The forgetting factor of the model  $\alpha$ .

In this article, the Interior-point method was used to optimize the parameters based on experimental data collection for the system for delays  $(t_d)$  ranging from 50 to 150 ms with the step size of 10 ms and upper bound frequency of harmonic kernels  $(\omega_b)$  from 1 to 5 Hz with the step size of 0.5 Hz. The

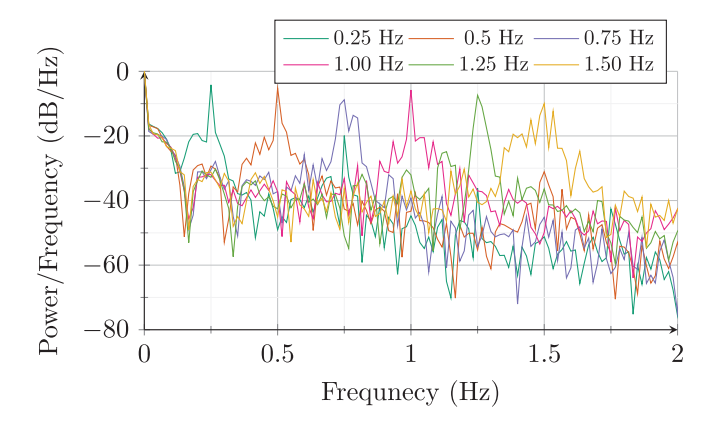


Fig. 5. Power spectrum density of the optimization input signals y(t). Each diagram shows the power spectrum density of each input signal.

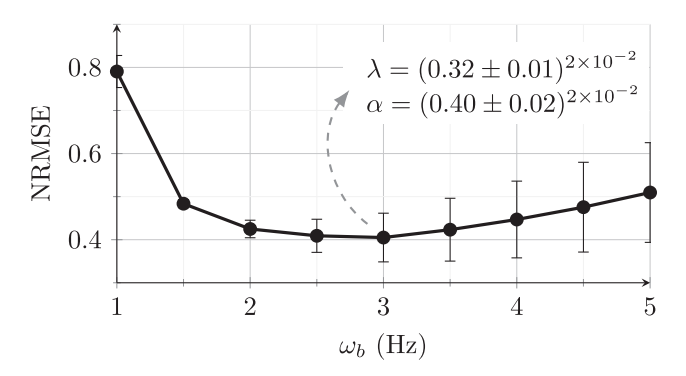


Fig. 6. Average of the normalized cost function for optimals  $\alpha$  and  $\lambda$  with respect to the upper bound of the frequency of harmonic kernels. Reported values are the average of normalized RMSE (NRMSE) for the different input signals and network delays.

input signal y(t), which has been used for the hyperparameters optimization procedure, was captured from six simulated 60-min rehabilitation tasks, which were conducted by a virtual reality system designed for robotic rehabilitation. Point-to-point reaching motion from home to target position was selected for the simulated rehabilitation task (see Figs. 12 and 15). The frequency of target switching ranged from 0.25 to 1.5 Hz generated using the virtual reality environment and the Quanser  $\mathrm{HD}^2$  robot. Fig. 5 shows the power spectrum density of the captured signals. The captured position signal has been chosen as the input signal for the optimization procedure.

Since the optimization may deviate from a convex formulation, each problem has been conducted with 40 random initial values in order to find the best solution.

Root mean square error (RMSE) has been chosen for the cost function of the optimization problem as

$$C_{\omega_b, t_d}(\alpha, \lambda) = \sqrt{\frac{1}{n} \sum_{t=0}^{n} \left( y_{L(\omega_b, t_d, \alpha, \lambda)}(t) - y(t) \right)^2}$$
 (14)

where  $t_d$  is the network delay,  $\omega_b$  is the upper bound frequency of harmonic kernels, and n is the number of samples.

Fig. 6 shows the optimization results. This figure demonstrates the average and the error bar shows the standard deviation of the normalized value of the cost function shown in (14). The

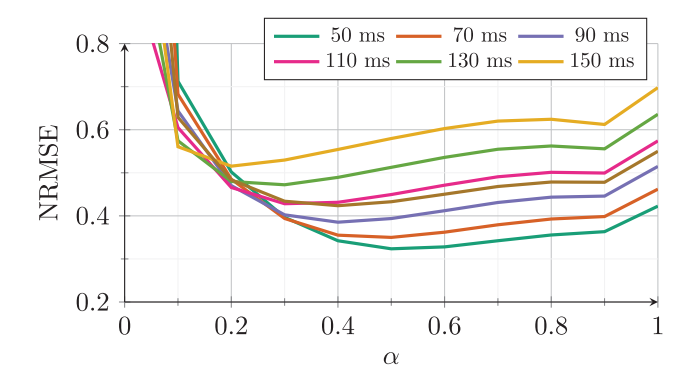


Fig. 7. Normalized cost function with respect to the model forgetting factor  $\alpha$  for different network delays. Reported values are the average of NRMSE for the different input signals.

average values are calculated using following equation:

$$ANC(\omega_b) = \frac{1}{66} \sum_{i=1}^{6} \sum_{j \in I} (NC_i(\omega_b, t_d))$$

$$I = \{50, 60, \dots, 150\}$$
(15)

where i represents the input signals, j is the network delay, and NC is the normalized cost function as follows:

$$NC(\omega_b, t_d) = \frac{C_{\omega_b, t_d}(\alpha, \lambda)}{\sqrt{\frac{1}{n} \sum_{t=0}^n (y(t - t_d) - y(t))^2}}$$
(16)

where  $\alpha$  and  $\lambda$  are the optimum values of the forgetting factors, calculated through optimization.

Fig. 6 shows that 3 Hz is the optimal value for the upper bound of the frequency window of the harmonic kernels. The calculated  $\alpha$  and  $\lambda$  for this window are  $(0.40\pm0.02)^{2\times10^{-2}}$  and  $(0.32\pm0.01)^{2\times10^{-2}}$ , respectively.

### A. Effect of Forgetting Factors and Regularization

The optimums  $\alpha$  and  $\lambda$  were determined through an optimization procedure along with  $\omega_b$ . In this section, an investigation has been done to demonstrate the effect of each forgetting factor and regularization factor on the output signal individually.

Fig. 7 shows the NRMSE with respect to the model forgetting factor  $\alpha$  for different network delays. In the experiment, the hyperparameters  $\omega_b$ ,  $\lambda$ , and  $\delta$  were selected to be 3, 0.32, and 0.1 Hz, respectively. As can be seen, the optimum value of  $\alpha$  depends on the network delay. The smaller the  $\alpha$ , the shorter is the memory of the system regarding Fourier coefficients. This leads to less contribution of the previously estimated coefficients resulting in abrupt changes in the estimations. On the other hand, the closer the value of  $\alpha$  to one, the higher is the contribution of the old coefficients in the estimation, resulting in sluggish behavior of estimation of the Fourier coefficients and less modeling accuracy.

The influence of  $\lambda$  on the output signal is shown in Fig. 8. The experiments were conducted with the hyperparameters  $\omega_b$ ,  $\alpha$ , and  $\delta$  to be 3, 0.4, and 0.1 Hz, respectively. The influence of  $\lambda$  on the output signal is almost similar to the effect of  $\alpha$ . Small  $\lambda$  increases the sensitivity of the RLS algorithm to recent

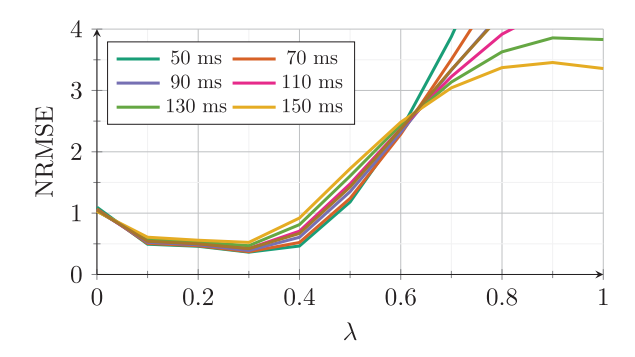


Fig. 8. Normalized cost function with respect to the correlation matrix forgetting factor  $\lambda$  for different network delays. Reported values are the average of NRMSE for the different input signals.

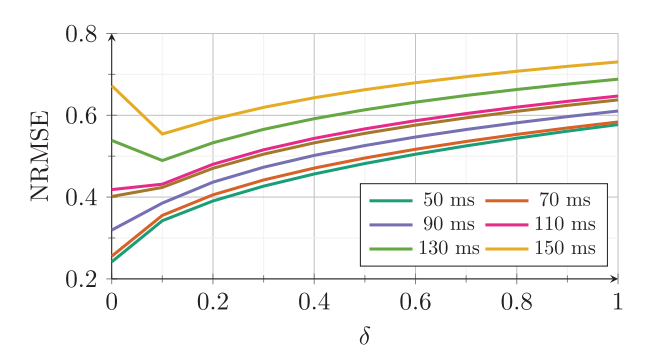


Fig. 9. Normalized cost function with respect to the RLS regularization factor  $\delta$  for different network delays. Reported values are the average of NRMSE for the different input signals.

values leading to fluctuations of the correlation matrix. However, a  $\lambda$  close to one results in the slow dynamics of the correlation matrix and higher estimation error.

Fig. 9 shows the effect of the regularization parameter on the output signal when  $\omega_b$ ,  $\lambda$ , and  $\alpha$  are 3, 0.32, and 0.4 Hz, respectively. The smaller the  $\delta$ , the smaller is the RLS regularization leading to large and high-frequency-estimated coefficients. This increases the estimation error, especially in larger network delays, because the high-frequency components encounter larger phase lag due to delay, making the BMFLC delay compensator sensitive to high-frequency components. On the other hand, large  $\delta$  increases the weight of the regularization term and pushes the estimated coefficients to zero, leading to larger modeling errors.

# B. Compensation Factor and Overcompensation

A compensation factor  $\xi > 0$  is introduced to the one-port BMFLC delay compensator to control the amount of reference signal shifting as

$$t_{\rm sh} = \xi t_d. \tag{17}$$

In this regard,  $0<\xi<1$  represents the undercompensation and  $\xi>1$  represents the overcompensation (shifting the signal in time more than the amount of delay). In this article, based on the conducted experimental results, the behavior of  $\xi$  from 0 to 2 was investigated to understand the effect of the compensation factor on the estimation error. Fig. 10 shows the NRMSE of the

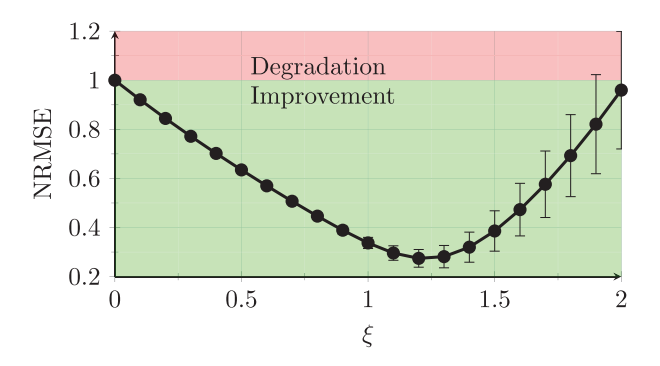


Fig. 10. NRMSE of the predicted signal with respect to the compensation factor  $\xi$ . Reported values are the average of NRMSE for ten different human input signals (duration = 30 s) with 100-ms delay.

compensated signal. The reported value is the average of the NRMSE for communication delay from 50 to 150 ms and input signal frequency from 0.25 to 1.50 Hz.

As shown in Fig. 10, the least estimation error has been achieved when  $\xi = 1.2$ . This observation suggests that a slight overcompensation of the delay can enhance the performance of the system. The main reason is due to low-pass filters in the system, which is added to compensate for the effects of sensor noises. In addition, possible slow variations in the Fourier's coefficients (due to the variation of the frequency content of the signal) may result in uncompensated harmonies in the reconstruction phase, the effect of which can be mitigated by slight overcompensation of the effect of delay, as seen in our experimental results. The compensation factor  $\xi$  adjusts the relative difference between the phase of the harmonic kernels and the Fourier coefficients. The higher the  $\xi$ , the larger will be the phase difference, thereby resulting in higher sensitivity of the compensator to high-frequency components of the signal and more distortion of the estimate. This is the reason for the increase in the variance of the NRMSE with an increase in  $\xi$ .

# V. MODULAR COMBINATION WITH STABILIZATION LAYER

An important aspect after modulating the signal using the proposed delay compensation layer is to guarantee the stability of the system. In this article, we propose a modular design, which allows for separating the transparency maximization (using the proposed delay compensator) and stabilization layers of the system.

In order to guarantee the stability of the system, an M-TDPC stabilizer has been implemented for the force wave reconstructed by the delay compensator [15]. M-TDPC observes the flow of energy, which may tend toward nonpassivity and will add enough damping to stabilize the system, taking into account the EoP of the user's limb. By placing the stabilizer after the delay compensator (see Fig. 15), the shortage of passivity (SoP) of the communication channel in addition to the potential SoP of the delay compensator will be monitored and compensated for using the M-TDPC algorithm, since the M-TDPC compensates for the SoP in the whole system and guarantees stability. In other words, any intervention of the proposed delay compensator will be validated considering the stability condition, using the M-TDPC algorithm on the fly.



Fig. 11. Experimental setup. Left: Quanser HD<sup>2</sup> haptic device. Right: Quanser rehabilitation robot.

Remark 5: It should be noted that no assumption on the passivity, linearity, or autonomous behavior (time-dependent) of the environment has been made in the R-BMFLC delay compensator formulation, and the stabilizer can stabilize the system for any environment.

#### VI. EXPERIMENTAL RESULTS AND DISCUSSION

In this section, the result and analysis of the effect of the delay compensator and its performance in the unilateral and the bilateral teleoperation system, as explained in Section V, are presented.

## A. Experimental Setup

Fig. 11 shows the experimental setup that has been used to verify the effect of the delay compensator in unilateral and bilateral teleoperation. The leader robot was a Quanser rehabilitation robot (by Quanser Inc.), and the follower robot was a Quanser HD² haptic device (by Quanser Inc.). The network between the robots was simulated and established in MATLAB Simulink. A virtual environment consisting of a 22-cm free motion and a viscoelastic wall with an impedance of  $Z_e=5+400/\mathrm{s}$  has been applied to the follower robot. This virtual environment simulates noncontact, in-contact, and the transition phase in teleoperation. The equation for the virtual environment is

$$f_e(t) = \begin{cases} 0 & p(t) < 22 & (18a) \\ 400(p(t) - 22) + 5\frac{d}{dt}p(t) \ p(t) \ge 22 & (18b) \end{cases}$$

where *p* is the distance of the end effector of the follower robot from the home position. A virtual reality system has been used to guide the operator through performing a predefined point-to-point task with different frequencies.

#### B. Unilateral Teleoperation

The R-BMFLC delay compensator has been applied to the motion signal in a unilateral teleoperation system to verify the corresponding performance (see Fig. 12). Ten random 1-D humanhand motion trajectories have been captured and fed to the communication channel with 100-ms network delay. The delayed signal  $y(t-t_d)$  is then fed to the delay compensation

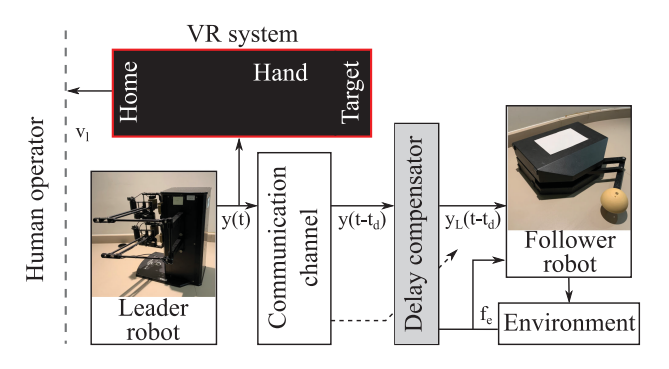


Fig. 12. Block diagram of the unilateral teleoperation system with R-BMFLC delay compensator.

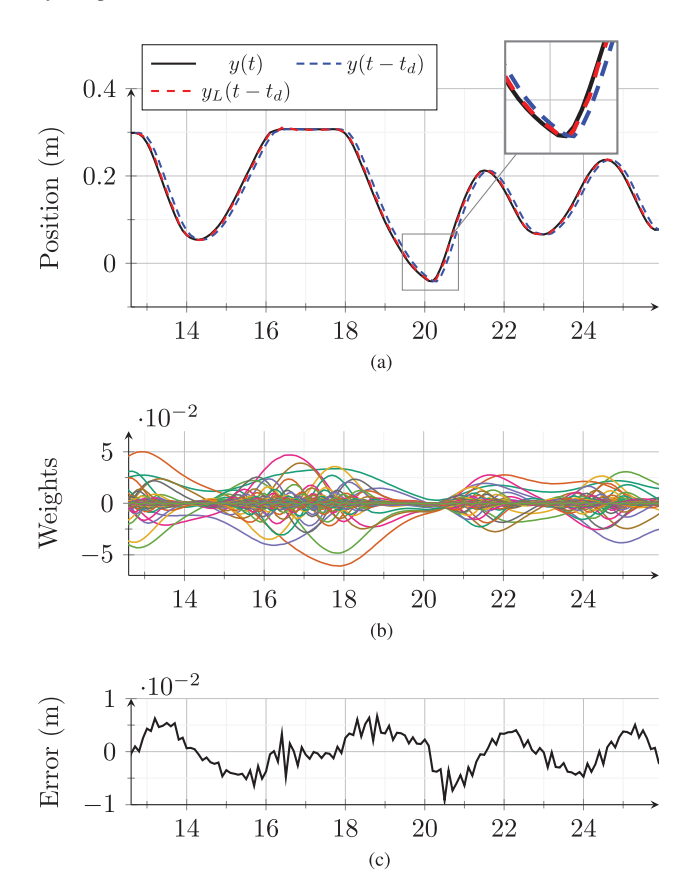


Fig. 13. Results of the unilateral delayed teleoperation with implemented delay compensator for a human hand motion trajectory signal. Communication delay is 100 ms. (a) Position signal before the communication channel, after the communication channel, and the compensated signal illustrating the eliminated phase lag. (b) Estimated weights of the R-BMFLCs. (c) R-BMFLC estimation error and delay compensator estimation error. Horizontal axes are time (s).

unit. The results for one captured motion signal are shown in Fig. 13.

Fig. 13(a) shows the input signal y(t) to the network, delayed signal  $y(t-t_d)$ , and compensated signal  $y_L(t-t_d)$ . As can be seen in the figure, the phase lag introduced by the network delay to the signal is eliminated, and the output of the compensator matches well with the signal that enters the communication channel.

Fig. 13(b) shows the Fourier coefficients estimated by the R-BMFLC. The stability of the weights vector and their responsiveness to the input signal confirm the efficacy of the

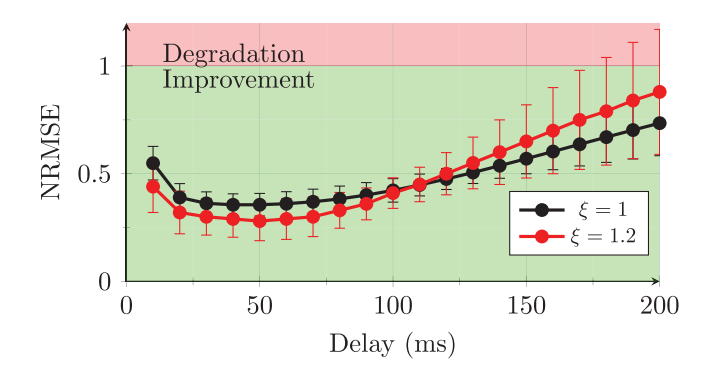


Fig. 14. NRMSE of delay compensated signal versus communication delay for two  $\xi$  values. Results are for one-port configuration.  $\xi = 1$  also shows the results for two-port configuration. Reported numbers are the average of ten different human input signals.

regulated cost function and forgetting memory along with their optimal tuning through optimization.

Fig. 13(c) shows the delay compensator estimation error. It can be seen that the compensator estimation error is within 0.01 m, which is around 3% of the amplitude of the position signal. It can also be seen from Fig. 13(c) that the compensator shows the highest error when the direction of the motion changes. This is because there are high-frequency components in the signal when the direction of motion changes, which leads to less estimation accuracy. However, the overall small estimation error validates the efficacy of the proposed approach.

A holistic analysis has been done on the estimation error of the delay compensator to demonstrate the effect of delay in the estimation accuracy. For this, the performance of the system was experimentally evaluated for a range of delays from 10 up to 200 ms. Fig. 14 shows the relation between NRMSE and communication delay for two compensation factors  $\xi = 1$  and  $\xi = 1.2$  for the one-port configuration. It should be noted that the results for the two-port configuration are the same as those for the one-port configuration when  $\xi = 1$ . As can be seen in the figure, the system performance was significantly improved using the proposed method. The result confirms the performance of the system for delays lower than 200 ms (one-way). For higher values of delay, the proposed compensation cannot enhance the performance, and this is due to exaggerated phase asynchrony between the compensated kernels and the variable Fourier coefficients during very long delays. Considering the existing internet technology, delay of 200 ms is technically very high and does not exist in a wide range of applications. As a result, the proposed method can cover a wide range of applications. Enhancing the performance of the system for very large delays (more than 200 ms) is one of the lines of our future work and can expand the applications for very slow communication.

### C. Bilateral Teleoperation

A telerobotic system with the MELFC control architecture has been implemented (see the schematic shown in Fig. 15). The delay compensator unit has been implemented in one-port and two-port configurations for the reflected force feedback signal to counteract the delay imposed by the communication channel on the force signal.

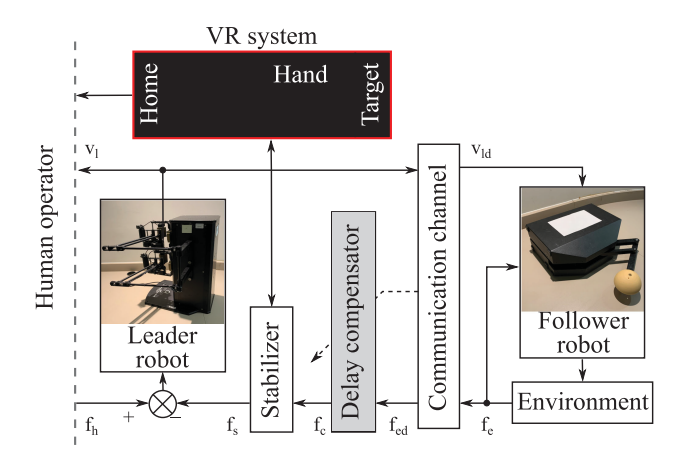


Fig. 15. Block diagram of the MELFC bilateral teleoperation system with R-BMFLC delay compensator and M-TDPC stabilizer.

Figs. 16 and 17 show the results for a haptics-enabled point-to-point task with 60-ms communication delay for one-port ( $\xi=1.2$ ) and two-port delay compensators, respectively. For the first 12 s, the system has been running when the proposed compensator was OFF. At t=12 s, the delay compensator was activated.

Figs. 16(a) and 17(a) show the environmental force and reflected force feedback to the leader robot. By comparing signals before and after the activation of the delay compensator, following two critical phenomena can be observed.

- 1) The phase lag of the reflected force feedback signal is eliminated using the proposed approach.
- The deviation of the reflected force due to the injected damping by M-TDPC stabilizer is significantly reduced, and the system exhibits improved force transparency.

It can be observed that the reflected force matches perfectly with the environmental force leading to ultimate force transparency even with delayed teleoperation. This can also be verified in Figs. 16(e) and 17(e), in which the absolute value of the force signal error in (19) is shown. The absolute value of the error is reduced drastically by 70% and 40% in one-port and two-port configurations, respectively, after the activation of the delay compensator.

Overshoots of the estimated signal can also be seen in Figs. 16(a) and 17(a) with the activation of the stabilizer. Although the overshoots are not significant in comparison to the amplitude of the signals, their influence on the perception of the environmental impedance by the human user will be investigated in future research.

$$e_{\text{force}}(t) = f_{\text{leader}}(t) - f_{\text{environment}}(t).$$
 (19)

Figs. 16(b) and 17(b) show the leader and follower velocity. Although the delay compensator is implemented for the force signal only, the corresponding indirect closed-loop effect on the velocity signal can be seen in the velocity signal. Less activation of the stabilizer is also seen (by 53% and 64% in one-port and two-port configurations, respectively), which leads to smoother velocity, as marked on the diagrams.

Figs. 16(c) and 17(c) show the input and output signal to the delay compensator representing the corresponding effect on the force signal. It can be concluded from the figure that the delay compensator adds phase lead to the signal and accurately counteracts communication delay.

The estimated Fourier coefficients by the R-BMFLC for the Fourier model are shown in Figs. 16(d) and 17(d). It has been observed that in the first 10 s (transient model population phase), the Fourier coefficients are fluctuating. However, the added regularization term and forgetting factor limits the coefficients prevented divergence.

Figs. 16(f) and 17(f) illustrates the activation of the M-TDPC stabilizer before and after the activation of the delay compensator. In order to keep the result in an observable range, the square root of the stabilizer's activation is reported. Less activation of the stabilizer by 53% and 64% for one-port and two-port configurations, respectively, with the implementation of the delay compensator show that the delay compensator has resulted in the lower SoP, which needed to be compensated by the stabilizer.

Fig. 18 shows the reflected force feedback (leader force) versus leader velocity for two point-to-point tasks with an active one-port R-BMFLC delay compensator and two same point-topoint tasks without delay compensator. This diagram shows the force feedback reflected to the operator versus their velocity. As shown in Fig. 1, under delay-free bilateral teleoperation, the sign of the slope of the reflected force should change with the change in the direction of motion. For example, at the onset of releasing phase, the force feedback starts to reduce, as expected when someone takes his/her hand out of the environment. This forms a round force-velocity diagram, as shown in Fig. 1. It should be noted that the intrinsic damping of the environment results in deviations from a perfect circle. The diagram gets an oblique oval shape in delayed teleoperation due to the added phase lag, which is significantly enhanced using the proposed approach.

In Fig. 18, it can be seen that the activation of the compensator has made the diagram smoother and closer to an ideal round shape. More specifically, the effect of the delay compensator can be seen in two parts of the figure, as explained in the following. First, the extra force and velocity fluctuations in the noncompensated graph are almost eliminated using the proposed approach, which is because of the less intervention of the M-TDPC stabilizer in the system. This is the same effect as marked in Fig. 16(a) and (b) and Fig. 17(a) and (b). Second, the reflected force reduces sooner after the start of the releasing phase. This is because of the compensation for the force signal delay (see the marked top-left area of Fig. 18). The abovementioned improvements in the force tracking lead to a better perception of the environmental impedance for the operator.

We also used a force error index, as defined in the following equation, for better demonstration of the effect of the delay compensator in the improvement of the force transparency. In this regard, we have

Force error index = 
$$\left(\int_0^n e_{\text{force}}^2(t)dt\right)^{0.5}$$
 (20)

where  $e_{\text{force}}$  is as in (19). In addition, we introduced the stabilizer's activation index as an indicator of the amount of the intervention imposed by the stabilizer in the teleoperation

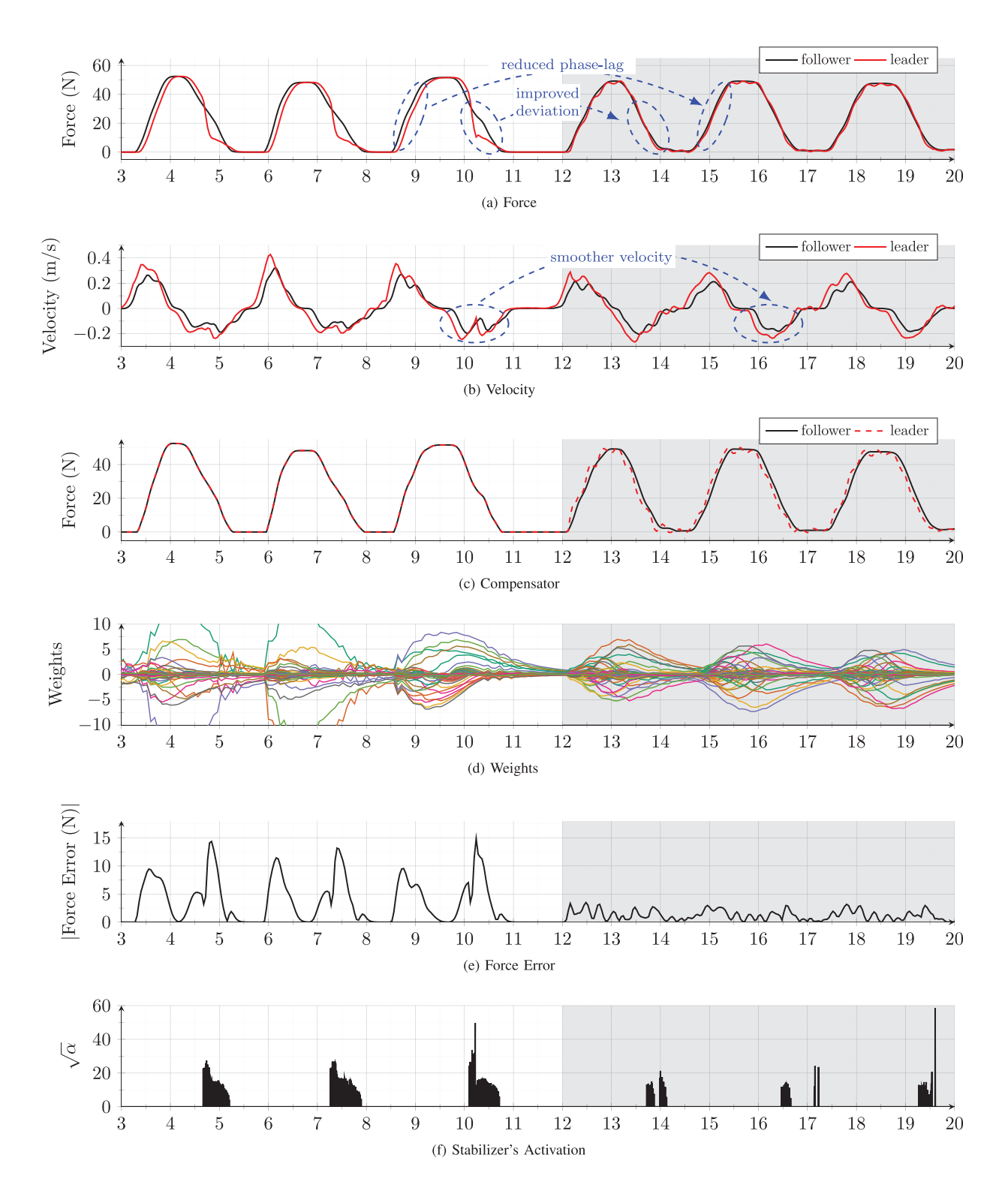


Fig. 16. Results of bilateral teleoperation using one-port delay compensator. The first 12 s demonstrate results when the delay compensator was deactivated. The delay compensator was activated from t=12 s to the end (the area shaded in gray) with  $\xi=1.2$ . (a) Environmental and leader force signals. It shows reduced phase lag and improved deviation of the leader force. (b) Leader and follower velocity. It demonstrates the increased smoothness of the velocity signal. (c) Input signal to delay compensator and compensated signal. (d) Estimated weight of the Fourier model. (e) Absolute error of the force signal, illustrating the improved force transparency. (f) Square root of the stabilizer's effort. Horizontal axes are time (s).

system as

Stabilizer's activation index = 
$$\int_0^n \alpha^2(t)dt$$
 (21)

where  $\alpha$  is the activation gain of the M-TDPC stabilizer. It should be noted that the lower value of both aforementioned indexes results in a more realistic perception of the environmental impedance for the operator. The mentioned parameters are used in the following experimental analysis.

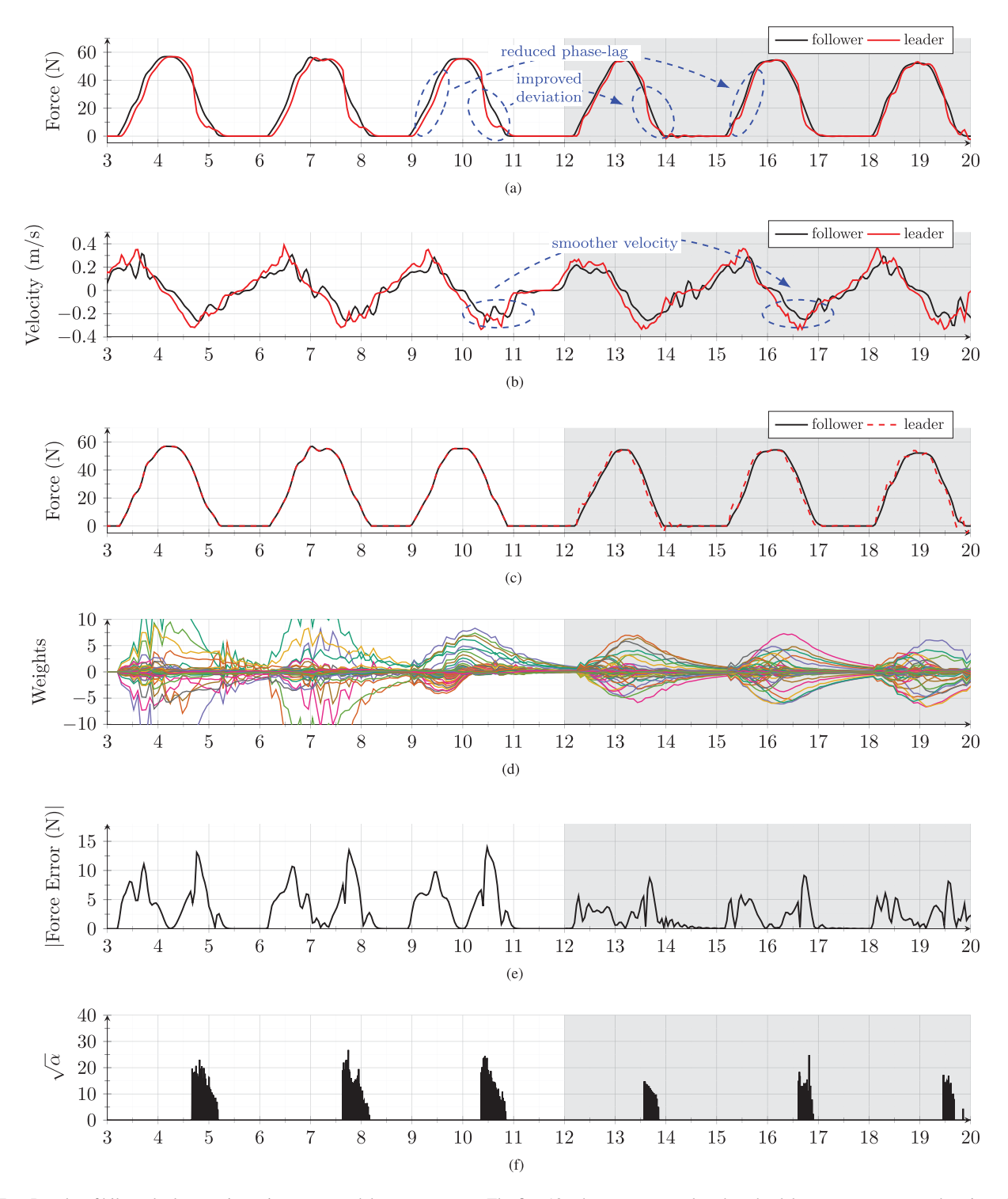


Fig. 17. Results of bilateral teleoperation using two-port delay compensator. The first 12 s demonstrate results when the delay compensator was deactivated. The delay compensator was activated from t=12 s to the end (the area shaded in gray). (a) Environmental and leader force signals. It shows reduced phase lag and improved deviation of the leader force. (b) Leader and follower velocity. It demonstrates the increased smoothness of the velocity signal. (c) Input signal to delay compensator and compensated signal. (d) Estimated weight of the Fourier model. (e) Absolute error of the force signal, illustrating the improved force transparency. (f) Square root of the stabilizer's effort. Horizontal axes are time (s).

Fig. 19(b) shows a holistic analysis of the performance of the system for one-port compensator under a variable communication delay that has been triangular wave with 60 ms minimum, 100 ms maximum, and 0.5-Hz frequency, as shown in Fig. 19(a). The percent of changes in the force error index and stabilizer's

activation index versus compensation factor  $\xi$  is shown. The minimum achieved percent of changes in force error index is -40% at  $\xi=1.2$ . The results conform with the results achieved in the unilateral teleoperation (see Fig. 10) and validates the performance of the proposed system. The percent of changes of the

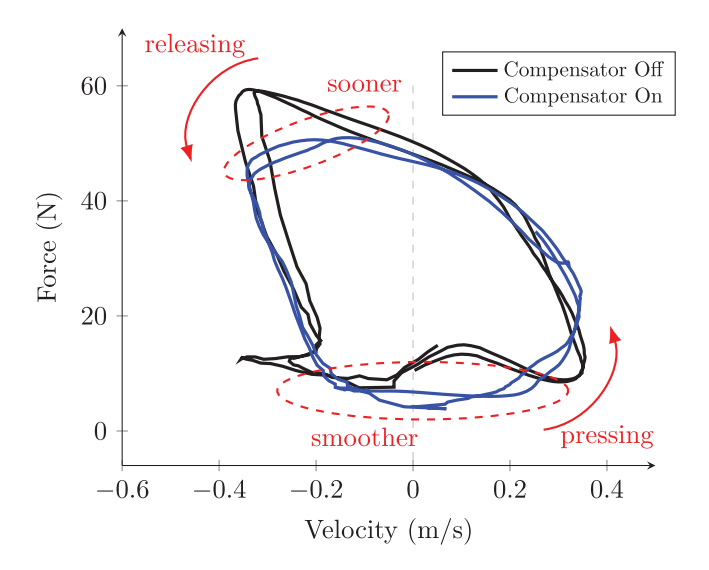


Fig. 18. Reflected force versus leader velocity when communication delay is 80 ms on each side. Black diagram: When the delay compensator is not active. Blue diagram: When delay compensator is active. The top-left-marked area illustrates the reduced relative phase lag of the reflected force with respect to the associated velocity. The bottom-marked area shows the smoother force and velocity due to less activation of the stabilizer.

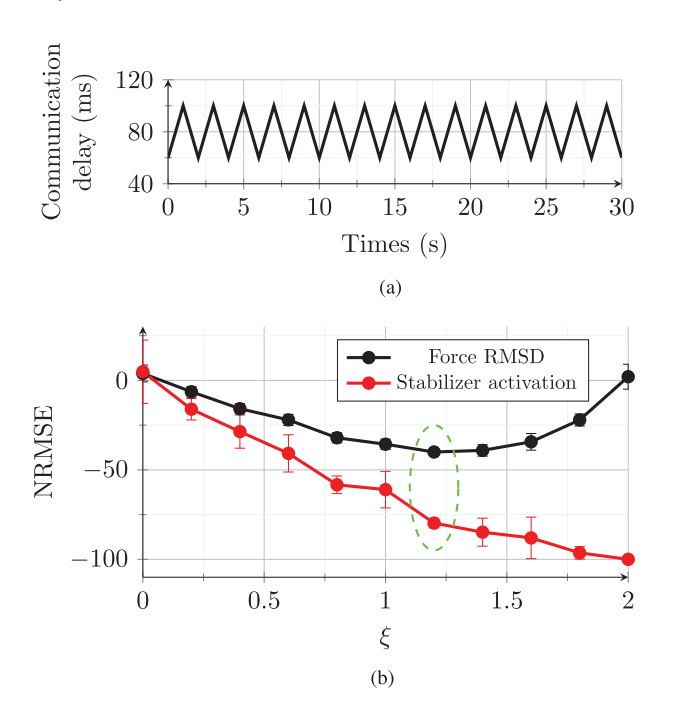


Fig. 19. (a) 30 s of one-way communication delay. (b) Percent of changes of force error index and stabilizer index versus compensation factor  $\xi$ . Communication delay has been variable triangular wave with 60 ms minimum, 100 ms maximum, and 0.5-Hz frequency.

average of stabilizer's activation index reduces with the increase of  $\xi$ . It gets to -79% at  $\xi=1.2$  and reaches close to -100% at  $\xi=2$ . This means that overcompensation for force signal also compensates for the existing delay of the velocity signal as well in the bilateral formulation. This phenomenon leads to less activation of the stabilizer. For the two-port configuration under the same delay condition, the force error index and the stabilizer's activation index were determined to be  $-32.4 \pm 2.3$ 

and  $-61.7 \pm 7.2$ , respectively. Close numbers to the values shown in Fig. 19(b) for  $\xi = 1$  verify that the performance of the two-port configuration is the same as the performance of the one-port configuration when  $\xi$  is equal to one.

As explained above, the best performance in terms of transparency improvement has been achieved using the one-port delay compensator when  $\xi = 1.2$ , which requires known network delay. In this article, it has been assumed that the communication delay is variable, but known for the one-port BMFLC delay compensator. However, in most cases, in reality, the network delay has to be estimated using the methods explained in [44]–[47]; therefore, delay estimation accuracy may affect the accuracy of the delay compensator. Investigation of the effect of delay estimation accuracy on the delay compensator is another line of future research. The result achieved using the two-port delay compensator, which does not require delay estimation, also showed transparency improvement both in terms of force error and mitigation of the stabilizer's activation. This method can be considered as an alternative when the estimation of the network delay is not accessible.

#### VII. CONCLUSION

In this article, a new wave prediction method was proposed based on signal modeling with an R-BMFLC frequency decomposer and two implementations were investigated. The predictor was used to counteract the communication delay in telerobotics. An optimization procedure was carried out based on a systematically designed experimental point-to-point tasks to calculate the best design parameters of the delay compensator. The performance of the delay compensator and the corresponding effect on bilateral teleoperation with M-TPDC stabilizer were verified through experimental validation. Experimental results showed that implementation of the delay compensator led to the elimination of the phase lag of the reflected force feedback. It was shown that the proposed system was able to enhance the force-velocity transparency profile, resulting in a smoother shape and a convex relationship, which subsequently led to better perceptual expectation of the user. In addition, the results showed that the stabilizer's activation could significantly drop by 79%, while the force tracking was improved. Furthermore, smoother velocity was observed due to the less activation of the stabilizer. The proposed delay compensator was designed to be modular and to be applicable for a wide range of telerobotic applications. Improving the compatibility of the proposed system with higher frequency signals and investigating the effect of the accuracy of the network delay estimation on the proposed delay compensator are the main areas of future research.

# REFERENCES

- J. Artigas et al., "KONTUR-2: Force-feedback teleoperation from the international space station," in Proc. IEEE Int. Conf. Robot. Automat., 2016, pp. 1166–1173.
- [2] S. Mehrdad, F. Liu, M. T. Pham, A. Lelevé, and S. F. Atashzar, "Review of advanced medical telerobots," *Appl. Sci.*, vol. 11, no. 1, 2021, Art. no. 209.
- [3] N. Feizi, M. Tavakoli, R. V. Patel, and S. F. Atashzar, "Robotics and AI for teleoperation, tele-assessment, and tele-training for surgery in the era of COVID-19: Existing challenges, and future vision," *Front. Robot. AI*, vol. 8, 2021, Art. no. 610677.

- [4] S. F. Atashzar, J. Carriere, and M. Tavakoli, "How can intelligent robots and smart mechatronic modules facilitate remote assessment, assistance, and rehabilitation for isolated adults with neuro-musculoskeletal conditions?," Front. Robot. AI, vol. 8, 2021, Art. no. 610529.
- [5] A. Talasaz, A. L. Trejos, and R. V. Patel, "The role of direct and visual force feedback in suturing using a 7-DoF dual-arm teleoperated system," *IEEE Trans. Haptics*, vol. 10, no. 2, pp. 276–287, Apr.–Jun. 2017.
- [6] S. F. Atashzar, M. Shahbazi, and R. V. Patel, "Haptics-enabled interactive neurorehabilitation mechatronics: Classification, functionality, challenges and ongoing research," *Mechatronics*, vol. 57, pp. 1–19, 2019.
- [7] N. Najmaei, P. Yadmellat, M. R. Kermani, and R. V. Patel, "Application of Magneto-Rheological fluid based clutches for improved performance in haptic interfaces," in *Proc. IEEE Int. Conf. Robot. Automat.*, 2014, pp. 832–837.
- [8] N. Najmaei, A. Asadian, M. R. Kermani, and R. V. Patel, "Magneto-Rheological actuators for haptic devices: Design, modeling, control, and validation of a prototype clutch," in *Proc. IEEE Int. Conf. Robot. Automat.*, 2015, pp. 207–212.
- [9] D. A. Lawrence, "Stability and transparency in bilateral teleoperation," IEEE Trans. Robot. Automat., vol. 9, no. 5, pp. 624–637, Oct. 1993.
- [10] K. Hashtrudi-Zaad and S. E. Salcudean, "Analysis of control architectures for teleoperation systems with impedance/admittance master and slave manipulators," *Int. J. Robot. Res.*, vol. 20, no. 6, pp. 419–445, 2001.
- [11] K. Hashtrudi-Zaad and S. E. Salcudean, "Transparency in time-delayed systems and the effect of local force feedback for transparent teleoperation," *IEEE Trans. Robot. Automat.*, vol. 18, no. 1, pp. 108–114, Feb. 2002.
- [12] S. F. Atashzar, M. Shahbazi, H. A. Talebi, and R. V. Patel, "Control of time-delayed telerobotic systems with flexible-link slave manipulators," in *Proc. IEEE/RSJ Int. Conf. Intell. Robots Syst.*, 2012, pp. 3035–3040.
- [13] A. Haddadi and K. Hashtrudi-Zaad, "Bounded-impedance absolute stability of bilateral teleoperation control systems," *IEEE Trans. Haptics*, vol. 3, no. 1, pp. 15–27, Jan.–Mar. 2010.
- [14] A. Jazayeri and M. Tavakoli, "Absolute stability analysis of sampled-data scaled bilateral teleoperation systems," *Control Eng. Pract.*, vol. 21, no. 8, pp. 1053–1064, 2013.
- [15] S. F. Atashzar, M. Shahbazi, M. Tavakoli, and R. V. Patel, "A passivity-based approach for stable patient-robot interaction in haptics-enabled rehabilitation systems: Modulated time-domain passivity control," *IEEE Trans. Control Syst. Technol.*, vol. 25, no. 3, pp. 991–1006, May 2017.
- [16] S. F. Atashzar, İ. G. Polushin, and R. V. Patel, "A small-gain approach for nonpassive bilateral telerobotic rehabilitation: Stability analysis and controller synthesis," *IEEE Trans. Robot.*, vol. 33, no. 1, pp. 49–66, Feb. 2017.
- [17] S. Thudi and S. F. Atashzar, "Discrete windowed-energy variable structure passivity signature control for physical human-(tele) robot interaction," *IEEE Robot. Automat. Lett.*, vol. 6, no. 2, pp. 3647–3654, Apr. 2021.
- [18] N. Feizi, S. Thudi, R. V. Patel, and S. F. Atashzar, "Time-domain passivity-based controller with an optimal two-channel lawrence telerobotic architecture," in *Proc. IEEE Int. Conf. Robot. Automat.*, 2021, pp. 3865–3871.
- [19] G. Niemeyer and J. J. E. Slotine, "Telemanipulation with time delays," *Int. J. Robot. Res.*, vol. 23, no. 9, pp. 873–890, 2004.
- [20] A. Aziminejad, M. Tavakoli, R. V. Patel, and M. Moallem, "Wave-based time delay compensation in bilateral teleoperation: Two-channel versus four-channel architectures," in *Proc. Amer. Control Conf.*, 2007, pp. 1449–1454.
- [21] A. Aziminejad, M. Tavakoli, R. V. Patel, and M. Moallem, "Transparent time-delayed bilateral teleoperation using wave variables," *IEEE Trans. Control Syst. Technol.*, vol. 16, no. 3, pp. 548–555, May 2008.
- [22] Z. Chen, F. Huang, W. Sun, and W. Song, "An improved wavevariable based four-channel control design in bilateral teleoperation system for time-delay compensation," *IEEE Access*, vol. 6, pp. 12848–12857, 2018.
- [23] B. Hannaford and J. H. Ryu, "Time-domain passivity control of haptic interfaces," *IEEE Trans. Robot. Automat.*, vol. 18, no. 1, pp. 1–10, Feb. 2002.
- [24] J. H. Ryu, D. S. Kwon, and B. Hannaford, "Stable teleoperation with time-domain passivity control," *IEEE Trans. Robot. Automat.*, vol. 20, no. 2, pp. 365–373, Apr. 2004.
- [25] J. H. Ryu, J. Artigas, and C. Preusche, "A passive bilateral control scheme for a teleoperator with time-varying communication delay," *Mechatronics*, vol. 20, no. 7, pp. 812–823, 2010.
- [26] M. Panzirsch, J. H. Ryu, and M. Ferre, "Reducing the conservatism of the time domain passivity approach through consideration of energy reflection in delayed coupled network systems," *Mechatronics*, vol. 58, no. 11, pp. 58–69, Nov. 2019.

- [27] J. Artigas, J.-H. Ryu, and C. Preusche, "Time domain passivity control for position-position teleoperation architectures," *Presence: Teleoperators Virtual Environ.*, vol. 19, no. 5, pp. 482–497, 2010.
- [28] V. Chawda and M. K. Omalley, "Position synchronization in bilateral teleoperation under time-varying communication delays," *IEEE/ASME Trans. Mechatronics*, vol. 20, no. 1, pp. 245–253, Feb. 2015.
- [29] G. Bianchini, J. Bimbo, C. Pacchierotti, D. Prattichizzo, and O. A. Moreno, "Transparency-oriented passivity control design for haptic-enabled teleoperation systems with multiple degrees of freedom," in *Proc. IEEE Conf. Decis. Control*, 2018, pp. 2011–2016.
- [30] O. A. M. Franco, J. Bimbo, C. Pacchierotti, D. Prattichizzo, D. Barcelli, and G. Bianchini, "Transparency-optimal passivity layer design for time-domain control of multi-dof haptic-enabled teleoperation," in *Proc. IEEE/RSJ Int. Conf. Intell. Robots Syst.*, 2018, pp. 4988–4994.
- [31] M. Franken, S. Stramigioli, S. Misra, C. Secchi, and A. Macchelli, "Bilateral telemanipulation with time delays: A two-layer approach combining passivity and transparency," *IEEE Trans. Robot.*, vol. 27, no. 4, pp. 741–756, Aug. 2011.
- [32] Y. Ye, Y. J. Pan, Y. Gupta, and J. Ware, "A power-based time domain passivity control for haptic interfaces," *IEEE Trans. Control Syst. Technol.*, vol. 19, no. 4, pp. 874–883, Jul. 2011.
- [33] I. Nisky, F. A. Mussa-Ivaldi, and A. Karniel, "A regression and boundary-crossing-based model for the perception of delayed stiffness," *IEEE Trans. Haptics*, vol. 1, no. 2, pp. 73–82, Jul.–Dec. 2008.
- [34] C. N. Riviere, R. S. Rader, and N. V. Thakor, "Adaptive cancelling of physiological tremor for improved precision in microsurgery," *IEEE Trans. Biomed. Eng.*, vol. 45, no. 7, pp. 839–846, Jul. 1998.
- [35] K. C. Veluvolu, U.-X. Tan, W. T. Latt, C. Shee, and W. T. Ang, "Ban-dlimited multiple fourier linear combiner for real-time tremor compensation," in *Proc. 29th Annu. Int. Conf. IEEE Eng. Med. Biol. Soc.*, 2007, pp. 2847–2850.
- [36] K. C. Veluvolu and W. T. Ang, "Estimation and filtering of physiological tremor for real-time compensation in surgical robotics applications," Int. J. Med. Robot. Comput. Assist. Surg., vol. 6, no. 3, pp. 334–342, 2010
- [37] K. C. Veluvolu, W. T. Latt, and W. T. Ang, "Double adaptive bandlimited multiple fourier linear combiner for real-time estimation/filtering of physiological tremor," *Biomed. Signal Process. Control*, vol. 5, no. 1, pp. 37–44, 2010
- [38] S. F. Atashzar, M. Shahbazi, O. Samotus, M. Tavakoli, M. S. Jog, and R. V. Patel, "Characterization of upper-limb pathological tremors: Application to design of an augmented haptic rehabilitation system," *IEEE J. Sel. Topics Signal Process.*, vol. 10, no. 5, pp. 888–903, Aug. 2016.
- [39] Y. Gao, S. Wang, J. Zhao, and H. Cai, "Estimation of pathological tremor by using adaptive shifting BMFLC based on RLS algorithm," in *Proc.* IEEE Int. Conf. Mechatronics Automat., 2013, pp. 569–574.
- [40] Y. Wang and K. C. Veluvolu, "Time-frequency decomposition of band-limited signals with BMFLC and Kalman filter," in *Proc. 7th IEEE Conf. Ind. Electron. Appl.*, 2012, pp. 582–587.
- [41] S. Tatinati, K. C. Veluvolu, S.-M. Hong, W. T. Latt, and W. T. Ang, "Physiological tremor estimation with autoregressive (AR) model and Kalman filter for robotics applications," *IEEE Sensors J.*, vol. 13, no. 12, pp. 4977–4985, Dec. 2013.
- [42] A. H. Sayed, Adaptive Filters. Hoboken, NJ, USA: Wiley, 2011.
- [43] S. Ciochina, C. Paleologu, J. Benesty, and A. A. Enescu, "On the influence of the forgetting factor of the RLs adaptive filter in system identification," in *Proc. Int. Symp. Signals, Circuits Syst.*, 2009, pp. 1–4.
- [44] L. De Vito, S. Rapuano, and L. Tomaciello, "One-way delay measure-ment: State of the art," *IEEE Trans. Instrum. Meas.*, vol. 57, no. 12, pp. 2742–2750, Dec. 2008.
- [45] J. Hua, Y. Cui, Y. Yang, and H. Li, "Analysis and prediction of jitter of internet one-way time-delay for teleoperation systems," in *Proc. 11th IEEE Int. Conf. Ind. Informat.*, 2013, pp. 612–617.
- [46] L. Hongyan, W. Hong, and G. Chao, "Internet time-delay prediction based on autoregressive and neural network model," in *Proc. Int. Conf. Commun.*, *Circuits Syst.*, 2006, pp. 1758–1761.
- [47] Z. Juanping and G. Xianwen, "Time-delay analysis and estimation of internet-based robot teleoperation system," in *Proc. Chin. Control Decis. Conf.*, 2009, pp. 4643–4646.
- [48] N. Hogan, "Controlling impedance at the man/machine interface," in Proc. IEEE Int. Conf. Robot. Automat., 1989, pp. 1626–1627.
- [49] C. Elisei-Iliescu, C. Stanciu, C. Paleologu, J. Benesty, C. Anghel, and S. Ciochină, "Robust variable-regularized RLS algorithms," in *Proc. Hands-Free Speech Commun. Microphone Arrays*, 2017, pp. 171–175.



Navid Feizi (Graduate Student Member, IEEE) received the B.Sc. degree from Shiraz University, Shiraz, Iran, in 2016, and the M.Sc. degree from the Sharif University of Technology, Tehran, Iran, in 2019, both in mechanical engineering. He is currently working toward the Ph.D. degree in mechatronics with the School of Biomedical Engineering, Western University, London, ON, Canada.

He is currently a Research Assistant with Canadian Surgical Technologies and Advanced Robotics (CSTAR), Lawson Health Research Institute, Lon-

don, ON, Canada. He is also a Trainee in effective systems for procedure specific healthcare simulation, CSTAR. His research interests include human–robot interactions, rehabilitation and surgical robotics, haptics, teleoperation, and smart actuators.



**Rajni V. Patel** (Life Fellow, IEEE) received the Ph.D. degree in electrical engineering from the University of Cambridge, Cambridge, U.K., in 1973.

He is currently a Distinguished University Professor and the Tier-1 Canada Research Chair with the Department of Electrical and Computer Engineering, Western University, London, ON, Canada, with cross appointments in the School of Biomedical Engineering, the Department of Surgery and the Department of Clinical Neurological Sciences. He is also the Director of Engineering, Canadian Surgical Technological T

gies and Advanced Robotics, Lawson Health Research Institute, London, ON, Canada

Dr. Patel is a Fellow of the ASME and the Royal Society of Canada and the Canadian Academy of Engineering. He was on the editorial boards of the IEEE TRANSACTIONS ON ROBOTICS, IEEE/ASME TRANSACTIONS ON MECHATRONICS, IEEE TRANSACTIONS ON AUTOMATIC CONTROL, Automatica, and Journal of Medical Robotics Research, and is currently on the editorial board of the International Journal of Medical Robotics and the Computer Assisted Surgery.



Mehrdad R. Kermani (Member, IEEE) received the Ph.D. degree in electrical and computer engineering from The University of Western Ontario, London, ON, Canada in 2005. He is currently a Professor with the Department of Electrical and Computer Engineering and the Director of Advanced Robotics and Mechatronic Systems Laboratory, Western University, London, ON, Canada. His expertise and research interests include humanrobot collaborations, robotic grasping, compliant actuations, agricultural robotics, and the use of smart materials for developing human-

centric technologies in robotics.

Dr. Kermani was the Co-Chair of a number IEEE conferences, including ICRA and the selection panel of multiple funding agencies. He is currently an Associate Editor for the IEEE ROBOTIC AND AUTOMATION LETTERS.



S. Farokh Atashzar (Senior Member, IEEE) received the Ph.D. degree in electrical and computer engineering from the University of Western Ontario, London, ON, Canada, in 2017. He is currently an Assistant Professor with New York University (NYU), New York, NY, USA, jointly appointed with the Department of Electrical and Computer Engineering and Mechanical and Aerospace Engineering. He is also affiliated with NYU WIRELESS, New York, NY, USA, and NYU Center for Urban Science and Progress, New York, NY, USA, and leads Medical

Robotics and Interactive Intelligent Technologies Lab, NYU, and the activities of the lab are funded by the US National Science Foundation. He was a Postdoctoral Scientist with Imperial College London, London, U.K. His research interests include a human machine interface, haptics, human-centered robotics, biosignal processing, deep learning, and nonlinear control.

Prof. Atashzar was the recipient of several awards, including the 2021 Outstanding Associate Editor of the IEEE ROBOTICS AND AUTOMATION LETTERS. He is an Associate Editor for the IEEE TRANSACTIONS ON ROBOTICS and IEEE ROBOTICS AND AUTOMATION LETTERS.